Correlation of a FSAE Prototype CFD to Wind Tunnel Experimental Data

Hugues PERRIN
Department of Aerospace Engineering, École de technologie supérieure, Montréal, Canada

Abstract

This paper details the methodology used by Formule ETS to correlate Computational Fluid Dynamics (CFD) simulations with wind-tunnel (WT) data for the 2025 race car DELTA-25. Wind-tunnel tests were performed at the Ford Motor Company facilities in Allen Park, Michigan, and provided force and balance measurements over a matrix of ride heights representative of on-track operation. The CFD setup was constructed to mirror the WT conditions, and a structured comparison procedure was implemented to align reference frames, non-dimensional coefficients, and post-processing steps. The methodology is evaluated through its ability to reproduce global aerodynamic loads and aero-balance trends. The final correlation yields an average discrepancy of approximately 4% in CLA, CDA and aero-balance across the relevant ride-height range, while providing similar, demonstrating that the proposed workflow provides a robust basis for simulation-driven aerodynamic development. This validation work enters a partnership agreement between Formule ETS and Ford Motor Company

Introduction

Computational Fluid Dynamics (CFD) has become a central tool in the aerodynamic development of FSAE race cars, enabling teams to explore design concepts at comparatively low cost and within tight time constraints. However, the usefulness of CFD as a decision-making tool is entirely dependent on the fidelity of the underlying models and the accuracy of the assumptions used in their setup. Geometric simplifications, turbulence modeling choices, mesh resolution, and boundary conditions can all introduce uncertainties that are difficult to quantify purely from numerical indicators such as residuals or mesh refinement studies. Without systematic experimental validation, there is a significant risk that CFD predictions will misrepresent absolute levels of downforce, drag, or aero-balance, leading to suboptimal or even detrimental design choices.

Wind-tunnel testing provides an essential experimental counterpart to CFD by delivering controlled, repeatable measurements of aerodynamic forces and moments over well-defined operating conditions. For FSAE prototypes, wind tunnels allow teams to investigate the influence of parameters such as ride height, pitch, yaw, and wing settings in an almost perfectly controlled and known situation. Moreover, WT facilities can be configured to approximate key aspects of the on-track environment—such as ground effect, blockage, and freestream turbulence—while offering a higher level of instrumentation and data quality than typical full-scale testing. When properly designed, a WT campaign yields a high-quality reference dataset against which numerical predictions can be rigorously assessed.

The combination of CFD and wind-tunnel testing is particularly valuable in the FSAE context, where resources, time, and testing opportunities are limited. Student teams often must rely on CFD to guide rapid iteration of wings, diffusers, and underbody geometries through the design season. In this environment, a validated CFD process can greatly reduce the number of physical prototypes required and focus limited testing time on the most promising configurations. Conversely, an unvalidated CFD workflow may still appear internally consistent while systematically over- or under-predicting key metrics such as lift coefficient, drag coefficient, or center of pressure location. Establishing a robust correlation between CFD and wind-tunnel data is thus a prerequisite for using simulation results as a reliable basis for concept selection, parameter sweeps, and sensitivity studies.

Beyond simply comparing force coefficients, a structured validation and correlation methodology enhances the overall engineering rigor of FSAE aerodynamic development. By enforcing consistency in reference quantities, boundary conditions, post-processing, and uncertainty estimation between CFD and experiments, teams can identify model deficiencies and quantify the remaining discrepancies in a transparent manner. This process not only improves confidence in the current design, but also creates a repeatable framework that can be reused and refined across successive vehicle generations. In the long term, such a methodology supports the transition from “CFD as a visualization tool” to “CFD as a validated, predictive tool” that underpins a professional-level aerodynamic development process within a student racing team.

Figure 1: DELTA-25 during the WT campaign, Allen Park MI, October 2025

Since 2023, Formule ETS has entered a partnership agreement with Ford Motor Company, based in the Detroit area, with the objective of increasing their knowledge and understanding of ground vehicles aerodynamics and apply it to their year round design processes to create innovative and efficient designs with the use of precise CFD models. [1]

FMC Wind Tunnel 8 Presentation

Wind Tunnel 8 (WT8), as described in SAE paper 2002-01-0252 [2] is part of Ford Motor Company's Driveability Test Facility (DTF) in Allen Park, Michigan, a complex conceived to move a significant portion of vehicle development from on-road testing to controlled laboratory environments. The overarching driver was the need to shorten development cycles while maintaining, or improving, product quality by enabling year-round testing of driveability, climate, and powertrain performance. Within this context, WT8 was added to provide a capability that existing facilities could not offer: the controlled reproduction of adverse wind–noise and aerodynamic phenomena that had previously been observed only sporadically on track under particular combinations of wind speed and ambient conditions. These issues tended to be discovered late in the program and were difficult to reproduce and engineer out using track testing alone, motivating the inclusion of a state-of-the-art aeroacoustic wind tunnel in what was originally envisioned primarily as a powertrain and climatic test facility.

WT8 is a ¾ open-jet, closed-return wind tunnel specifically designed to combine aerodynamic, aeroacoustic, climatic, and powertrain testing in a single installation, in line with the design philosophy of other modern full-scale automotive and aeroacoustic facilities. [3, 4, 5, 6] The primary nozzle has an area of 18.7 m² with a contraction ratio of 6:1 and a maximum speed of 54 m/s; an interchangeable 10.5 m² insert increases the contraction ratio to 10.7:1 and allows testing up to 67 m/s. The tunnel circuit incorporates carefully designed diffusers, turning vanes, and a cross-leg heat exchanger, with extensive acoustic treatment on walls, ceilings, corners and collector flaps to achieve low background noise while maintaining good flow quality. [7] The open-jet plenum is lined to provide hemi-anechoic conditions down to about 100 Hz, and commissioning results demonstrate dynamic pressure uniformity on the order of 0.25 %, flow angularity below 0.1°, and very low longitudinal turbulence levels in the core flow, consistent with best practices for open-jet automotive wind tunnels. [8, 9] A six-component external balance with a 6.7 m-diameter turntable and an integrated 2-wheel dynamometer (250 kW absorption) completes the test section equipment, enabling combined aerodynamic, aeroacoustic and powertrain measurements under controlled climatic conditions.

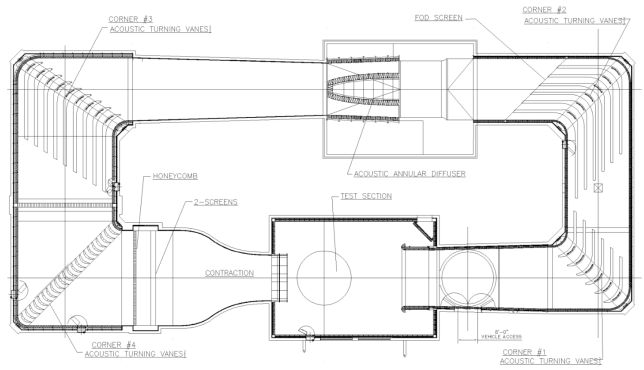

Figure 2: Wind Tunnel 8 layout - SAE Paper 2002-01-0252

A key feature of WT8 for ground-vehicle testing is its boundary layer control (BLC) system, implemented as a tangential blowing slot immediately downstream of the nozzle exit. The system is modeled after the DNW moving-ground concept [10, 11] and is designed to reproduce displacement thicknesses representative of moving-belt simulations, with nominal targets of $\delta^* \approx 8$ mm for full-scale vehicles and $\delta^* \approx 4$ mm for scale-model testing. [7, 12] Air is extracted from the main circuit upstream of the fan, compressed, and delivered to a plenum beneath the test-section floor before being discharged through a 1 mm-high slot, allowing the effective displacement thickness of the floor boundary layer to be driven to a few millimeters or effectively to zero at the user's discretion. Commissioning measurements with boundary-layer rakes and iterative calibration of plenum pressure versus test-section speed showed that the system can reliably impose prescribed δ^* levels over the balance region. This capability is particularly important for correlating road-vehicle CFD to wind-tunnel data, as it allows the underbody flow and diffuser performance to be assessed under conditions that closely approximate a moving ground, thereby improving the representativeness of measured forces and moments for race-car and high performance cars applications. [7]

The Boundary Layer Control system should be highly regarded when building a CFD model of the Wind Tunnel case.

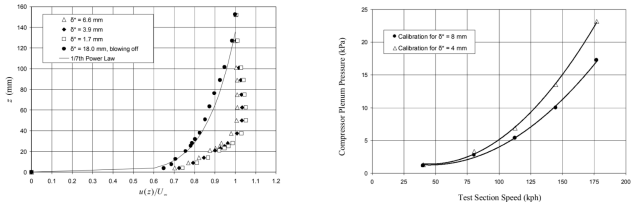

Figure 3: BLC System velocity profiles at centerline @ 177km/h test section speed (left) and typical calibration curves (right) - SAE Paper 2002-01-0252

As part of its ongoing collaborations and student partnership programs with engineering universities, Ford Motor Company regularly hosts leading North American Formula SAE teams such as RIT Racing from the Rochester Institute of Technology (2024 FSAE Electric champions) and Formule ETS from École de Technologie Supérieure (2023 FSAE Electric champions), to evaluate their aerodynamic devices and vehicle models in WT8. Testing FSAE-scale prototypes in a facility originally conceived for full-scale road vehicles, however, presents specific challenges and necessitates dedicated preparatory work before entering the test section. These preliminary studies and adaptations, encompassing both hardware and test methodology, prove to be critical in achieving a high level of correlation between numerical predictions and wind-tunnel measurements.

Figure 4: DELTA-25 with wheel wake replication devices and ground clearance adjusting wheels strapped to WT8 balances with FSAE adapters

Since 2023, Formule ETS has been testing its Europe and North America title-winning cars in Ford Motor Company's WT8 facility to correlate CFD simulations with experimental data and improve the relevance of its aerodynamic models to on-track conditions. This collaboration has enabled the team to deepen its understanding of aerodynamics in an FSAE context while reinforcing design decisions through systematically acquired, data-driven evidence. Over the course of three wind-tunnel campaigns on three different vehicles, the discrepancy between CFD predictions and wind-tunnel measurements has been reduced from more than 40% to approximately 4% across the key aerodynamic metrics of interest.

Preliminary Preparations

This section will elaborate on the different designs used to increase the fidelity of the wind tunnel test case, to compensate for non-rotating wheels, non-moving ground and balance adapters. This section will also cover the test plan for the 2025 WT correlation campaign.

Wheel Wake replication

In the aerodynamic testing of open-wheel prototypes, the wake generated by rotating wheels represents one of the most critical factors, as it strongly influences the performance of any aerodynamic device located downstream. This effect is particularly significant for FSAE vehicles, where compact packaging and tightly coupled aerodynamic elements make the flow topology around the wheels especially sensitive. However, WT8 is an aeroacoustic facility and does not incorporate a moving-belt system to simulate a rolling road and, consequently, true rotating-wheel conditions. To address this limitation, a dedicated wheel-flow control device was designed and tested, intended to reproduce the boundary-layer separation and flow behavior around the wheel that would be observed under realistic on-track operating conditions.

This device takes the shape of forward facing multi-flaps placed on each front and rear wheels to affect any elements downstream of the wheels and subsequent turbulators.

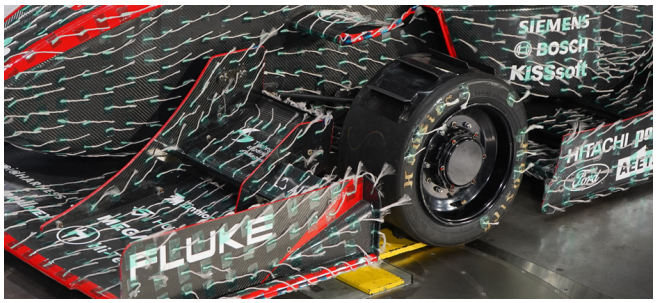

Figure 5: Wheel Wake Turbulators on DELTA-25's Front-Left wheel

The simple 3D-printable design allows for an easy replacement should in-test failure occur, while offering a reasonable similarity in wheel wake effects.

The figure 6 below represents the wheel wake effects during a realistic moving ground + rotating wheel case on a Y-plane placed at the centerline of the wheel. A separation zone is visible starting just before the top of the wheel's tire with a large high-pressure flow downstream of the wheel. Figure 7 highlights the comparison of the same wheel

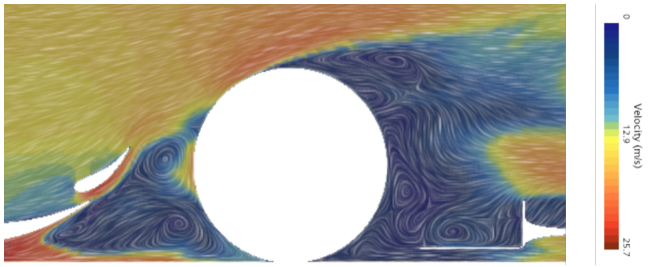

Figure 6: Wheel Wake around MANIC-24's wheel in track conditions

wake for WT8 conditions, namely without a moving ground and rotating wheels, for a clean wheel and a wheel with wheel wake replication devices. Those figures feature the same color scheme as the figure 6 for clearer understanding.

Numerically, the wheel wake replication devices featured in figure 7 increased the drag by 17% compared to a clean wheel for WT8 conditions, lowering the difference in drag between WT8 conditions and track conditions below 5%. However, the difference in lift forces (i.e downforce) remain strongly different due to a much lower ground effect on a non-moving ground and unfortunately couldn't be taken into consideration to further validate the fidelity of the presented wheel wake replication.

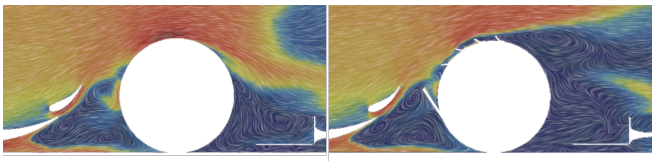

Figure 7: Wheel Wake around MANIC-24's wheel in WT8 conditions with (right) and without (left) wheel wake replication devices

Ground clearance and Ride Heights conformation

During the first WT campaign of Formule ETS in 2023, a lack of fidelity and relevancy to track conditions arose due to the necessity of balance adapters. Due to being an industrial wind tunnel designed around common road cars, FSAE prototypes with wheel dimensions of 1143 x 1525 millimeters fall short of the adaptability range of WT8, creating the need for adapters. Those adapters induce an increase of around 30 millimeters in ride height leading to unrealistic ground clearance and irrelevant test cases.

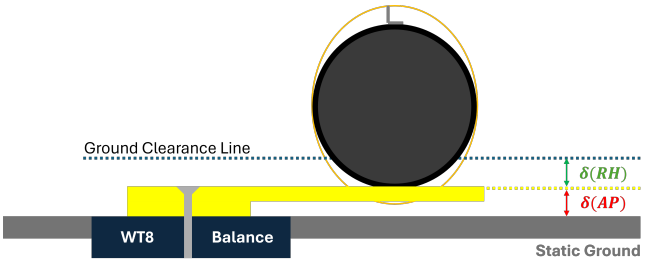

Figure 8: Schematic of the 2023 WT8 situation with increased ride heights

Figure 8 and 9 illustrate the strapping method in WT8 for the MANIC-23 campaign as well as the increase in ride height ($\delta(AP)$) induced by the adapter plates. The wheel is strapped to the adapter plate with a ratchet strap around the full tire. An aluminum L-shape is placed on top of the tire for wheel wake replication purposes.

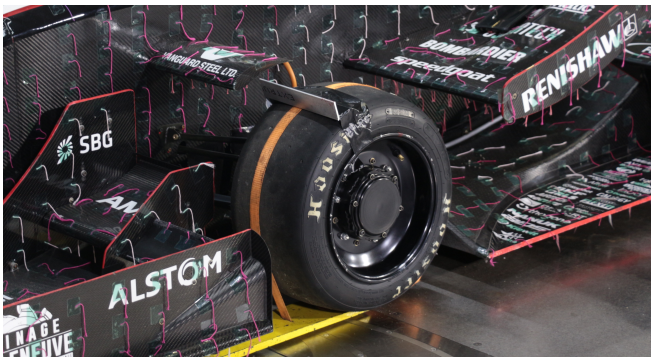

Figure 9: Photograph of MANIC-23's wheel strapped to the adapter plate

From 2024 onwards, the problem was solved by modifying a set of tires exclusively for WT8 testing purposes. This was achieved by cutting out holes so the ratchet strap now goes around the wheel rim instead of the tire. Moreover, the bottom side of the tire has been cut off and replaced by 3D printed blocks that subtracts $\delta(AP)$ from the total ride height of the car and places the car at the originally wanted ground clearance. The schematic of the situation is subject of the figure 10.

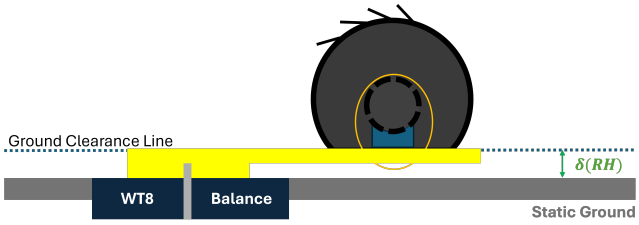

Figure 10: Schematic of the 2025 WT8 situation with corrected ride heights

This corrected setup proved to be more reliable to measure aerodynamic effects around an FSAE for the track driving envelope and increased the understanding around ground-effect based aerodynamic devices.

Tufting and flow visualization

In automotive aerodynamics, tufting refers to a surface-flow visualization technique in which small yarn tufts are attached to the vehicle body and observed via still images or video to infer local flow direction, separation, and unsteadiness. On full-scale passenger cars, dense tuft arrays combined with image-processing algorithms allow quantitative extraction of tuft orientation and thus separation/reattachment patterns and unsteady flow phenomena, providing far more information than purely qualitative inspection. [13] For open-wheeled race cars and FSAE-type prototypes, tufts are routinely used alongside CFD and other flow-visualization techniques (e.g. smoke) to interpret underbody and diffuser performance and to diagnose discrepancies between numerical and wind-tunnel results. [14] Modern automotive wind-tunnel test guidelines explicitly list tufting as a standard surface-flow visualization method for both production vehicles and race cars, on par with oil-flow and PIV-based approaches that are far more expensive nonetheless. [15]

Figure 11: Tufts arranged to capture the boundary layer separation on the rear wing endplate of DELTA-25

Tufts, particularly in our case, represent a more graphic way of visualizing and validating our CFD models by comparing the areas where the boundary layer is separated or not from the wall, along validating local flow directions.

Planning of the campaign

The planning of the campaign (see annex 1) was driven by the validation of existing simulation tools, in particular the general-purpose straight-line model [1] and the cornering aerodynamics model [16]. In total, twelve wind-tunnel runs were conducted, each comprising multiple operating points designed to populate the validation space for these models.

To enable a direct comparison between wind-tunnel measurements and on-track operating conditions, modifications were made to the prototype's suspension so that the test-section ride heights (RH) would correspond to dynamic rather than purely static values. This was achieved by replacing the springs and dampers with rigid members and locking the rockers, thereby constraining the car in heave and roll and ensuring a well-defined geometric configuration for each prescribed RH setting.

Run 0 was devoted to facility and fixture checkout. The vehicle was exposed to the envelope of test speeds and yaw angles to verify the structural integrity of the mounting system and to confirm that the prototype remained secure under the most adverse anticipated conditions. Runs 1 and 2 were then used to assess Reynolds-number independence over the relevant speed range and, simultaneously, to generate a first set of reference data points for subsequent CFD comparison.

Runs 3, 4 and 5 targeted the validation of the cornering aerodynamics model. Asymmetric loading conditions representative of steady-state cornering were imposed by introducing roll angles of 0°, 0.5° and 1°, corresponding approximately to lateral accelerations from 0 g to 1.5 g. With the exception of a dedicated yaw-stability run, yaw angles were kept small so as to mirror the cornering yaw levels measured on track using slip-angle sensors. Runs 6 through 11 focused on the straight-line model validation by systematically sweeping the ride heights configurations typically used on track at different speeds, thereby increasing the density of available correlation points.

Run 12 was designed to verify the structural integrity of the aerodynamic devices at the theoretical maximum speed of the planned 2026 prototype. All wind-tunnel conditions were subsequently reproduced in CFD, and the resulting force and moment predictions were compared to the measurements to identify potential modeling deficiencies and to quantify the reliability of the simulation framework.

Finally, Run 13 was dedicated to qualitative flow visualization. Smoke and laser-plane techniques were employed to study vortex generation and the overall flow structures around the car, with particular attention to the regions surrounding the radiator inlets and exits, the underbody, and the wing-tip vortices. This run was also the opportunity to simulate pilot head movements and their influence on rear wing efficiency and flow structure.

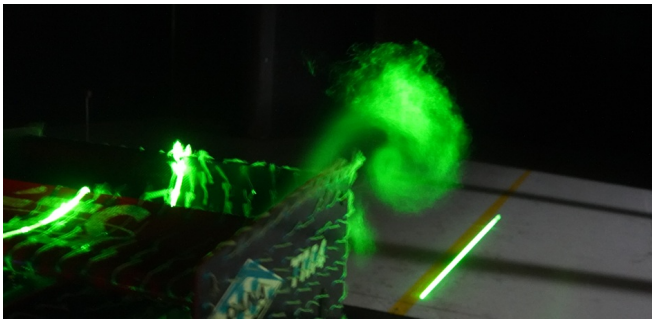

Figure 12: Smoke and laser visualization of the rear endplate vortex

Simulation Setup

Wind Tunnel Simulation

[REDACTED FROM PUBLIC VERSION]
[SEEK CONTACT FOR FURTHER INFORMATION]

General Purpose Track Models

SEE REFERENCE N° FETS-2024-02 [1]
SEE REFERENCE N° FETS-2024-03 [16]

The general purpose track models were the subject of different papers. The modifications of the models brought by this wind tunnel campaign are included in these references. Further modeling and validation details are also covered in these references.

Results and Analysis

Demonstrating Reynolds-number independence is a prerequisite for meaningful correlation between CFD, wind-tunnel measurements, and on-track performance. Aerodynamic forces and flow structures—such as separation, transition, and vortex formation—are generally functions of the Reynolds number, so if the flow remains Reynolds-sensitive within the tested range, discrepancies between CFD and experiments may simply reflect differences in Reynolds number rather than deficiencies in the modeling or test setup. The Reynolds number is defined by

$$\mathrm{Re} = \frac{\rho V L}{\mu}$$

By showing that global quantities such as lift, drag, and aero-balance vary only weakly over the relevant Reynolds-number range, one can justify using a "compromise" test speed or scale while still claiming that the results are representative of the operational regime. This, in turn, ensures that residual differences between CFD and wind-tunnel data can be attributed to geometry, boundary conditions, or turbulence modeling choices, thereby enabling a more reliable calibration and validation of the simulation framework. In particular, applications to subsonic incompressible flows prove the existence of a clear Reynolds threshold for which aerodynamical coefficient cease to vary until compression effects start to take place. Reynolds independence typically happens for speed upwards of 12 to 16 meters per second.

Quantities of interests include the coefficients of lift, drag and side force per unit area. All three are equally defined by the equations :

$$x = \tfrac{1}{2}\,\rho\,V^2\,C_A \;\mid\; C_A = \frac{2x}{\rho V^2}$$

where C_A applies to $C_L A$, $C_D A$ and $C_S A$ and x is the relevant force

We also define ABX and ABY as the pressure center coordinates along the X and Y axis. Aerobalance is also mathematically defined as

$$ABX = \frac{F_{zF}}{F_z} = \frac{M_{yR} \cdot L}{F_z}$$

Other quantities of interest include per-wheel vertical loads and moments along every axis of the vehicle. These quantities will not be mentioned here since they're purely performance focused and less about model validation.

Figures 13 and 14 show the relations between aerodynamic coefficients (CLA, CDA) and Reynolds (via air velocity).

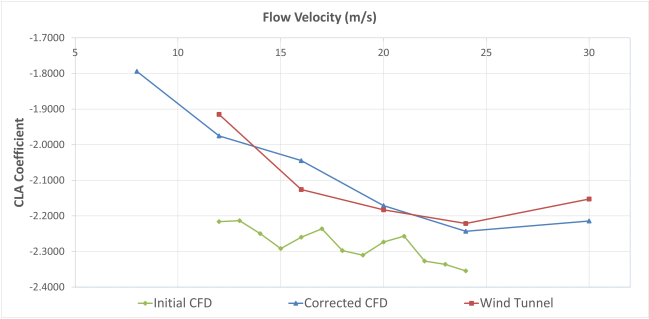

Figure 13: CLA against Air Velocity - Comparison between initial and corrected CFD models, and experimental data

Initial CFD modeling showed an over-prediction of the produced downforce on wind tunnel testing conditions. Model review proved lack of refinement in critical areas of the mesh and further tuning of the solvers and equations led to a corrected CFD model achieving an average deviation of 2.28% (8.04% for initial modeling) for the CLA coefficient, and an average deviation of 1.88% (4.32%) for the CDA coefficient.

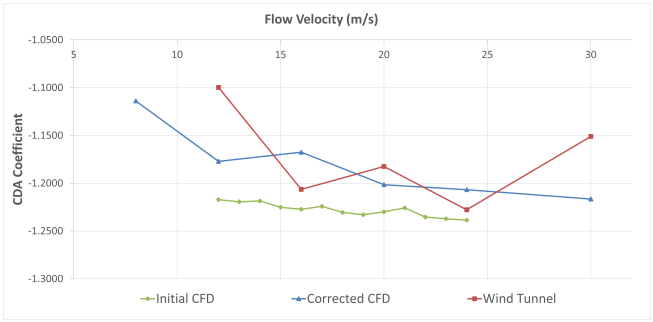

Figure 14: CDA against Air Velocity - Comparison between initial and corrected CFD models, and experimental data

The corrected model proves reliable predictions for aerodynamic coefficients when used with WT-like boundary conditions and outside of Reynolds-dependent ranges. Extension to track conditions are covered thereafter as well as in the FETS-2024-02 [1] reference.

The second phase of the test plan focused on asymmetric conditions and examined the variation of the vehicle's aerodynamic characteristics under combined yaw and roll, as encountered predominantly during on-track cornering.

The graphic thereafter sums up the variations in CLA for a yaw sweep for a neutral roll angle. Variations of CDA due to yaw angle however fell under negligible thresholds and are not plotted.

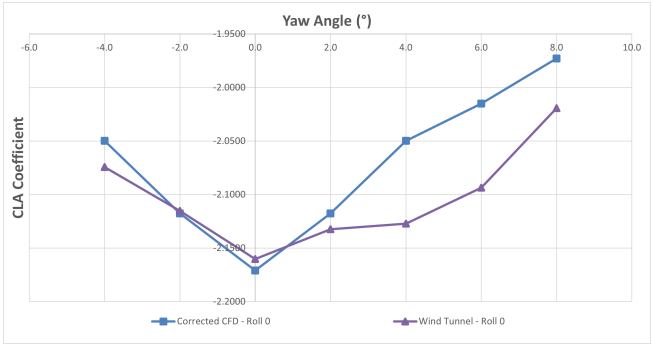

Figure 15: CLA against Yaw angle @ 16m/s air velocity and neutral roll

The corrected CFD model shows great correlation to experimental data, especially for yaw angles inferior to 2 degrees. For higher yaw angles, the differences between simulation and experimental results increases although following the same tendency. Moreover, differences between negative and positive yaw angles in experimental data are to be noted, highlighting a potential lack of fidelity of the symmetrical model. Those differences are principally explained by a poor manufacturing precision of the prototype. The precision of the model is however sufficient for cornering applications as vehicle sideslip rarely exceeds 2 to 3 degrees under transient cornering experimental data. The average deviation between simulation results and experimental data reaches 3.58% for the CLA coefficient while the CDA coefficient presents an average deviation of 3.05%.

Non-neutral roll angles of 0.5 degrees and 1 degree are also applied for a shorter yaw sweep to study the influence or rolling during cornering situations. Combined roll-yaw setups aim at reproducing cornering conditions at realistic lateral accelerations. Lateral accelerations and cornering slip angles were measured during track testing and implemented into a vehicle dynamics model [16] to compute accurate value couples.

Figure 16: CLA against Yaw angle @ 16m/s air velocity

The corrected CFD model slightly under-predicts downforce prediction under cornering conditions. However, tendencies are highlighted and comparable between simulation and wind tunnel data for yaw and roll influence. This study would benefit from a greater number of points, especially more roll setups, to further improve the understanding of the cornering cases.

The introduction of asymmetric aerodynamic conditions makes the presence of a lateral force component, acting along the vehicle body y-axis, explicitly apparent. This side force arises whenever the flow sees the car under non-zero yaw and/or roll, breaking the left–right symmetry of the baseline configuration. As shown in figure 17, the magnitude of the lateral force increases with yaw angle and is further modulated by roll angle, reflecting the combined influence of crossflow and load transfer on the distribution of pressure and vortex structures around the vehicle. This behavior is directly relevant to on-track cornering and crosswind scenarios.

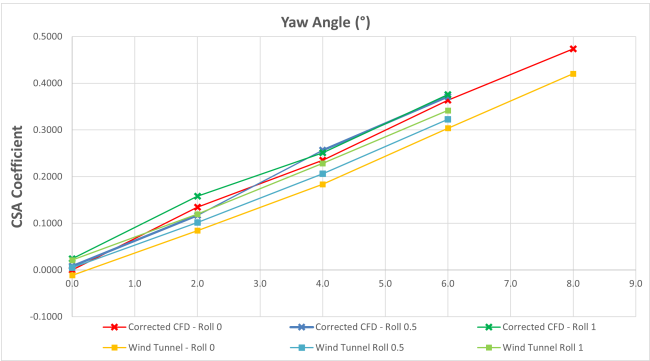

Figure 17: CSA against Yaw angle @ 16m/s air velocity and different roll angles

Although the CFD model over-predicts the magnitude of the forces by an average of 17.15% over all cases relative to the wind-tunnel data, it nonetheless captures the main aerodynamic trends, with side force increasing approximately linearly with yaw angle and exhibiting a modest rise at higher roll angles. The relatively large deviation in absolute level is attributed to the small side-force magnitudes involved in these highly transient conditions, combined with suboptimal anisotropic mesh refinement in the regions governing lateral load generation.

Finally, Runs 6 through 11 aimed at establishing aero-maps linking front ride height and rear ride height to aerodynamic quantities. From a CFD standpoint, these points also tested the CFD model's robustness to vehicle dynamics setup changes. Each run tested a different setup under three velocity settings to provide averaged aerodynamic coefficient for increased fidelity. Missing points were approximated through a bi-quadratic interpolation for which the R^2 is displayed next to the table. Anchor values are displayed in bold characters.

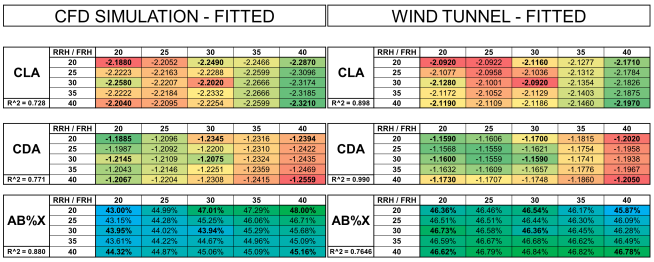

Figure 18: Interpolated CFD and WT Aeromaps for CLA, CDA and ABX

The fitted aero-maps show that CFD and wind-tunnel data are strongly correlated in trend but not in absolute levels, with some notable differences in aero-balance sensitivity. For both CLA and CDA, CFD and experimental data predict essentially the same qualitative dependence on ride heights. Increasing RRH leads to a monotonic increase in downforce magnitude and drag for both WT data and CFD, and the effect of FRH is similar: higher FRH generally produces more negative CLA and slightly higher CDA. The location of the high-downforce, high-drag corner of the map is therefore between CFD and WT data, which is a key argument towards physical plausibility and model correlation.

Quantitatively, however, the CFD model is systematically stronger. Across the matrix, CFD CLA and CDA are typically stronger than the wind-tunnel CLA and CDA. This bias is fairly uniform in the CLA and CDA maps as the differences between CFD and WT do not change sign or exhibit large local anomalies, which suggests that a simple offset or scaling could bring force levels into closer agreement without distorting the present trends. The higher R^2 values for the wind-tunnel fits in CLA and CDA (0.898 and 0.990 for WT vs 0.728 and 0.771 for CFD) also indicate that the experimental response surface is smoother and more internally consistent than the CFD one, particularly for lift, translating to a robust and relevant interpolation, while the R^2 values downwards of 0.8 for the CFD fit provide a less robust, although sufficient, interpolation.

A more detailed comparison between CFD results and WT data is the subject of figure 19.

	RRH / FRH	20	25	30	35	40
CLA	20	-4.59%	-5.40%	-6.29%	-5.59%	-5.34%
	25	-5.44%	-5.75%	-5.95%	-6.04%	-6.02%
	30	-6.11%	-5.74%	-5.26%	-6.14%	-6.18%
	35	-4.96%	-5.38%	-5.69%	-5.90%	-5.99%
Avg = -5.54%	40	-4.01%	-4.67%	-5.04%	-5.31%	-5.64%

	RRH / FRH	20	25	30	35	40
CDA	20	-2.55%	-4.22%	-5.51%	-4.24%	-3.11%
	25	-3.62%	-4.61%	-4.98%	-4.73%	-3.88%
	30	-4.70%	-4.76%	-4.18%	-4.97%	-4.16%
	35	-3.53%	-4.63%	-5.10%	-4.95%	-4.19%
Avg = -4.30%	40	-2.87%	-4.25%	-4.77%	-4.68%	-4.22%

	RRH / FRH	20	25	30	35	40
AB%X	20	7.25%	3.16%	-1.01%	-2.43%	-4.64%
	25	7.22%	4.79%	2.56%	0.52%	-1.35%
	30	5.95%	5.50%	5.22%	2.50%	1.30%
	35	6.40%	5.25%	4.31%	3.56%	3.01%
Avg = 3.92%	40	4.93%	4.10%	3.80%	3.70%	3.46%

Figure 19: Difference between CFD and WT Aeromaps

Larger discrepancies can be seen on the ABX aero-map, highlighting the poor fidelity of the model to correctly predict the aerodynamic balance effects of the car. In fact, CFD modeling struggles to replicate even wind tunnel trends CFD predicts that aero-balance shifts significantly with ride height, whereas the WT measurements indicate that the real car maintains a nearly constant front load share. For design purposes, the present CFD model is not representative of functioning conditions and cannot be used to predict aerodynamic balance despite an absolute average deviation of 3.92%.

As for CLA and CDA, the low, constant, deviation (averaging 5.54% for CLA, 4.30% for CDA) provides a solid foundation for global aerodynamic forces prediction. The constant difference across the ride height range hints at an underlying parameters damaging the fidelity of the global forces.meli

Finally, considering the wind tunnel operation parameters, the magnitudes seen in these aero-maps are not representative of DELTA-25's track performance due to the absence of powerful ground effects representing close to a third of the total downforce produced. However the corrected model established through that wind tunnel campaign can be adapted to simulate real track conditions and build according aero-maps that should be compared to track-issued experimental data for further correlation of the model. Preliminary work towards that correlation showed a high responsiveness of the model in comparison to downforce data extracted from suspension mounted load cells, with a precision allowing for fine tuning of the dynamics setup.

Conclusion

Through several means, we have proved the high correlation between wind-tunnel provided experimental data and a corrected CFD model, achieving a high fidelity in predicting the aerodynamic effects of a FSAE open-wheel prototype. That strongly correlated model should now be used for design and performance purposes by Formule ETS and aligns with the professional standards of the team.

Recommendation

First, the model would benefit from targeted mesh refinement in regions responsible for side-force generation, a recommendation that is particularly critical for cornering studies, where lateral loads increase and should be exploited to improve FSAE vehicle performance by the implementation of vertical force-producing elements.

Second, the nearly constant offset between wind-tunnel data and CFD predictions for CLA and CDA suggests an issue related to geometric simplification. Prior work indicates that an oversimplified inboard wheel model can increase CLA and CDA by 3–7% compared with a more detailed hub model. Correcting this should theoretically further reduce the gap between simulation and experimental data.

Finally, WT8's BLC system introduces a complex inlet setup for the CFD model. Further wind tunnel testing should be conducted with and without this system to quantify and conclude on its influence on FSAE open-wheel cars.

References

1. H. Perrin and E. Houri, *Straight Line Simulation Model Towards FSAE Aerodynamics*. Formule ETS, 2024.
2. J. Walter, E. Duell, B. Martindale, S. Arnette, P. A. Nagle, W. Gulker, S. Wallis, and J. Williams, "The driveability test facility wind tunnel no. 8," *SAE Technical Paper*, no. 2002-01-0252, 2002.
3. R. M. Allen and D. H. Reed, "Development of the boeing low speed aeroacoustic facility (lsaf)," in *14th DGLR/AIAA Aeroacoustics Conference*, no. DGLR/AIAA 92-02-030, (Aachen, Germany), 1992.
4. G. Wickern and N. Lindener, "The audi aeroacoustic wind tunnel: Final design and first operational experience," *SAE Technical Paper*, no. 2000-01-0868, 2000.
5. R. Künstner, J. Potthoff, and U. Essers, "The aero-acoustic wind tunnel of stuttgart university," *SAE Technical Paper*, no. 950625, 1995.
6. M.-S. Kim, J.-H. Lee, J.-D. Kee, and J.-H. Chang, "Hyundai full scale aero-acoustic wind tunnel," *SAE Technical Paper*, no. 2001-01-0629, 2001.
7. E. Mercker and H. W. Knape, "Ground simulation with moving belt and tangential blowing for full-scale automotive testing in a wind tunnel," *SAE Technical Paper*, no. 890367, 1989.
8. J. Hoffman, B. Martindale, S. Arnette, J. Williams, and S. Wallis, "Effect of test section configuration on aerodynamic drag measurements," *SAE Technical Paper*, no. 2001-01-0631, 2001.
9. S. A. Arnette, T. D. Buchanan, and M. Zabat, "On low-frequency pressure pulsations and static pressure distribution in open jet automotive wind tunnels," *SAE Technical Paper*, no. 1999-01-0813, 1999.
10. German-Dutch Wind Tunnel (DNW), "Aero-acoustic check-out of DNW," Tech. Rep. DNW-TM-80.002, DNW, Feb. 1980.
11. J. C. A. van Ditshuizen, G. D. Courage, R. Ross, and K. J. Schultz, "Acoustic capabilities of the german-dutch wind tunnel dnw," in *21st AIAA Aerospace Sciences Meeting*, no. AIAA 83-0146, (Reno, NV, USA), 1983.
12. H. Schlichting, *Boundary-Layer Theory*. New York: McGraw-Hill, 7 ed., 1979.
13. D. Wieser, S. Bonitz, L. Löfdahl, A. Broniewicz, C. N. Nayeri, C. O. Paschereit, and L. Larsson, "Surface flow visualization on a full-scale passenger car with quantitative tuft image processing," *SAE Technical Paper*, no. 2016-01-1582, 2016.
14. N. Dyverfors, T. Fernberg, M. Juhlin, and T. Larsson, "Interaction of downforce generating devices and cooling air flow – a numerical and experimental study on open wheeled race cars," *SAE Technical Paper*, no. 2012-01-1165, 2012.
15. F. Wittmeier, A. Bianco, J. Bratby, K. Howard, T. Roper, and V. Senft, "CAATS – automotive wind tunnel test techniques," *SAE Technical Paper*, no. 2024-01-2543, 2024.
16. H. Perrin and E. Houri, *Aerodynamic Simulation of a FSAE Open-Wheel Car During Cornering*. Formule ETS, 2024.

Definitions, Acronyms, Parameters

BLC	Boundary Layer Control
CFD	Computational Fluid Dynamics
DTF	Driveability Test Facility
FMC	Ford Motor Company
FSAE	Formula Society of Automotive Engineers
(R/F)RH	(Rear/Front) Ride Height
WT	Wind Tunnel

ABX	Aerobalance along longitudinal axis (in %)
ABY	Aerobalance along lateral axis (in %)
CDA	Coefficient of Drag per unit Area (in m^{-2})
CLA	Coefficient of Lift per unit Area (in m^{-2})
CSA	Coefficient of Side force per unit Area (in m^{-2})
$F_?$	Force along an axis (in N)
L	Reference Length / Wheelbase (in m)
$M_?$	Moment around an axis (in $N \cdot m$)
V	Velocity (in $m \cdot s^{-1}$)
ρ	Fluid Density (in $kg \cdot m^{-3}$)
μ	Dynamic Viscosity (in $Pa \cdot s$)

Contact Information

Hugues PERRIN, M.Sc
contact@huperrin.com

APPENDIX 1 - Wind Tunnel Test Plan

Test Conditions

Run WT	Configuration	Point	V_{inf} (m/s)	Vinf (kph)	FRH (mm)	RRH (mm)	Roll (°)	Pitch (°)	Yaw (°)	Notes	Time
0	Check data point	1									16h58
1	Straight Speed Sweep	1	8	28.8	30	30	0.0	0.0	0.0		17h10
	30 - 30	2	12	43.2	30	30	0.0	0.0	0.0		
		3	16	57.6	30	30	0.0	0.0	0.0		
		4	20	72	30	30	0.0	0.0	0.0		
		5	24	86.4	30	30	0.0	0.0	0.0		
		6	30	108	30	30	0.0	0.0	0.0		
		END									17h30
2	Straight Speed DRS Sweep	1	12	43.2	30	30	0.0	0.0	0.0		17h35
	30 - 30	2	16	57.6	30	30	0.0	0.0	0.0		
		3	20	72	30	30	0.0	0.0	0.0		
		4	30	108	30	30	0.0	0.0	0.0		
		END									17h46
3	Yaw Stability	1	16	57.6	30	30	0.0	0.0	4.0		17h51
	30 - 30	2	16	57.6	30	30	0.0	0.0	2.0		
		3	16	57.6	30	30	0.0	0.0	-2.0		
		4	16	57.6	30	30	0.0	0.0	-4.0		
		5	16	57.6	30	30	0.0	0.0	-6.0		
		6	16	57.6	30	30	0.0	0.0	-8.0		
		7	20	72	30	30	0.0	0.0	-8.0		
		8	20	72	30	30	0.0	0.0	-6.0		
		9	20	72	30	30	0.0	0.0	-4.0		
		10	20	72	30	30	0.0	0.0	-2.0		
		END									18h23
4	Cornering (Roll 0.5)	1	16	57.6	30	30	0.5	0.0	0.0		18h35
	30 - 30	2	16	57.6	30	30	0.5	0.0	-2.0		
		3	16	57.6	30	30	0.5	0.0	-4.0		
		4	16	57.6	30	30	0.5	0.0	-6.0		
		END									18h47
5	Cornering (Roll 1.0)	1	16	57.6	30	30	1.0	0.0	0.0		18h54
	30 - 30	2	16	57.6	30	30	1.0	0.0	-2.0		
		3	16	57.6	30	30	1.0	0.0	-4.0		
		4	16	57.6	30	30	1.0	0.0	-6.0		
		END									19h06
6	Aeromap Setup 1	1	16	57.6	20	20	0.0	0.0	0.0		19h12
	20 - 20	2	20	72	20	20	0.0	0.0	0.0		
		3	24	86.4	20	20	0.0	0.0	0.0		
		END									19h19
7	Aeromap Setup 2	1	16	57.6	20	40	0.0	0.8	0.0		19h32
	20 - 40	2	20	72	20	40	0.0	0.8	0.0		
		3	24	86.4	20	40	0.0	0.8	0.0		
		END									19h39
8	Aeromap Setup 3	1	16	57.6	40	40	0.0	0.0	0.0		19h47
	40 - 40	2	20	72	40	40	0.0	0.0	0.0		
		3	24	86.4	40	40	0.0	0.0	0.0		
		END									19h56
9	Aeromap Setup 4	1	16	57.6	40	20	0.0	-0.8	0.0		20h12
	40 - 20	2	20	72	40	20	0.0	-0.8	0.0		
		3	24	86.4	40	20	0.0	-0.8	0.0		
		END									20h20
10	Aeromap Setup 5	1	16	57.6	30	20	0.0	-0.4	0.0		20h26
	30 - 20	2	20	72	30	20	0.0	-0.4	0.0		
		3	24	86.4	30	20	0.0	-0.4	0.0		
		END									20h35
11	Aeromap Setup 6	1	16	57.6	20	30	0.0	0.4	0.0		20h46
	20 - 30	2	20	72	20	30	0.0	0.4	0.0		
		3	24	86.4	20	30	0.0	0.4	0.0		
		END									20h58
12	High Speed	1	36	129.6	30	30	0.0	0.0	0.0		21h09
											21h11
13	Smoke Vis	1	Min		30	30	0.0	0.0	0.0		21h19
		END									22h34
END											22h34

Figure 20: Testing Plan used for the 2025 WT8 Campaign of Formule ETS